



Nickel and/or platinum modified crystalline silicon–carbon composites and their electrochemical behaviour towards the hydrogen evolution reaction

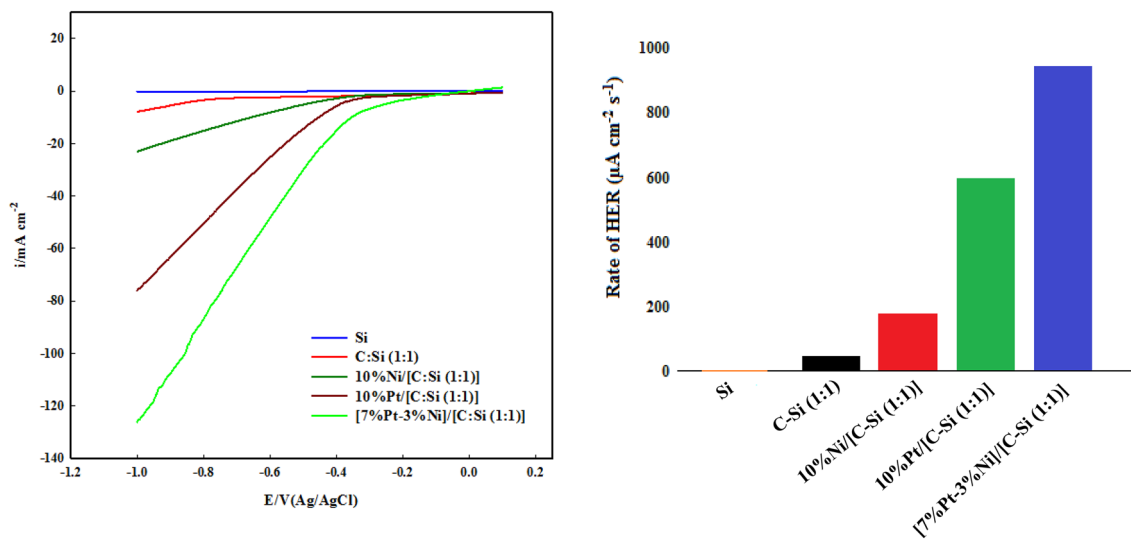
Merna N. Elsodany¹ · M. A. Abdel Rahim¹ · Nasser H. Shalaby² · M. A. Sultan¹

Received: 22 April 2023 / Accepted: 9 September 2023 / Published online: 5 October 2023
© The Author(s) 2023

Abstract

Generation of hydrogen is very important, as it is one of the most desired alternatives to fossil fuels. Moreover, designing of cheap and stable electrocatalysts is the task for the efficient generation of hydrogen with reasonable activity. Materials hybridization can be considered a tool for engineering different material properties. Composites of modified silicon such as C–Si, Ni/(C–Si), Pt/(C–Si), and Pt–Ni/(C–Si) were prepared (in weight percent) and studied as electrocatalysts for the hydrogen evolution reaction (HER) in 0.5 M H₂SO₄ solution. The surface morphologies and chemical compositions of the composites were confirmed using transmission electron microscopy (TEM), scanning electron microscopy (SEM), energy-dispersive X-ray analysis (EDX), X-ray photoelectron spectroscopy (XPS), X-ray diffraction (XRD), X-ray fluorescence analysis (XRF), elemental mapping, and BET surface analysis. The electrochemical measurements of linear sweep voltammetry (LSV), Tafel plots, chronoamperometry, and electrochemical impedance spectroscopy (EIS) were used to study the behaviour of the prepared electrodes toward the hydrogen evolution process. Among the various prepared composites, [7%Pt–3%Ni]/[C–Si (1:1)] composite shows the best catalytic activity with the highest HER rate (940.95 $\mu\text{A cm}^{-2} \text{ s}^{-1}$), the lowest overpotential [0.358 V vs. (Ag/AgCl) \approx 0.161 V vs. (RHE)] at 10 mA cm⁻², and the lowest charge transfer resistance (2.657 Ω) compared to other prepared electrodes. In addition, it gives the highest values of $4.219 \times 10^{-3} \text{ s}^{-1}$ turn over frequency (TOF) and 642 mA g⁻¹ mass activity. It shows good stability towards the hydrogen evolution reaction as the current density reaches about 34.28 mA cm⁻² after 5 h.

Graphical abstract



Extended author information available on the last page of the article

Keywords Silicon composites · C–Si · Ni/(C–Si) · Pt/(C–Si) · Pt–Ni/(C–Si) · Hydrogen evolution reaction

1 Introduction

The majority of energy is supplied by fossil fuels, but their long-term use is unacceptable. Therefore, increasing interest has been paid to renewable energy sources because of the energy crisis and environmental contaminants [1, 2]. To meet the demand for energy supply in the framework of a sustainable society, it becomes necessary to produce electricity from renewable energy sources [3].

Hydrogen is considered to be one of the most important future sources of clean energy because it is one of the most desired alternatives to fossil fuels [4–12]. The generation of hydrogen economically and sustainably is very important to the future realization of the hydrogen economy. The electrocatalytic hydrogen evolution reaction (HER) has attracted great interest because of its ease and generality [2, 5, 13–19]. Using renewable energy sources to produce hydrogen via electrolysis is a promising carbon-free method, but it must be improved in terms of efficiency and durability before it can be commercially viable [20–22].

Long-term stability of HER catalysts is of great importance for the material that has potential practical applications, especially considering that the HER catalyst mostly works in the acidic environment [13, 23, 24]. The key issue for HER is to search for cheap electrocatalysts with excellent activity in order to produce hydrogen massively and efficiently [13, 25–27]. Thus, designing stable catalysts that work well in an acidic environment is of great significance [28, 29].

It is well known that the interaction between the metal and the support materials may greatly influence the catalytic performance [30, 31]. Silicon (Si) and silicon-related materials are used in various applications, including solar cells and current electric devices [2, 32, 33]. Silicon supports have attracted much attention because of their novel physical and electrochemical properties. Several methods have been developed for the fabrication of Si, such as a laser-ablation metal-catalytic method [34], an oxide-assisted method [35, 36], and a solution technique [37, 38]. Si has several benefits, including low cost, abundance, nontoxicity, and well-understood processing methods. Also, it is relatively cathodically stable, has a suitable band gap resulting in the formation of an electrochemically passive oxide upon interaction with aqueous media, and in principle can produce a significant portion of the total photovoltage needed for water splitting [21, 39]. Functionalization of Si nanostructures is one way to further improve the properties of these devices. The chemical bonds between Si and metals prevent the

aggregation of the loaded metal nanoparticles [40, 41], which could greatly enhance the electrocatalytic stability.

Carbon Black Vulcan XC 72 is one of the commonly used conducting supports in the preparation of catalysts, where it showed good properties such as porous nature, light weight, large surface area, and good adsorption of the catalyst on its surface [42]. They possess high electrical conductivity, high chemical stability, and extremely high mechanical strength and modulus [43]. Accordingly, they were applied and used as supports in electrocatalysis [44, 45].

Platinum (Pt) is regarded as the best catalyst with the highest efficiency at the current stage. Because of their high current densities and near-zero overpotential, Pt and Pt-based materials have been widely used as HER catalysts [14, 46–50]. The high cost and rareness of Pt have motivated scientists to design new materials as acceptable replacements for Pt or to contain as little Pt as possible [48]. So, adding a small amount of platinum to other metals is preferred to avoid the high cost of platinum and obtain the advantages of the synergy of the added metals.

Ni is considered an efficient and stable electrocatalyst for producing hydrogen in an alkaline medium [51, 52]. By adjusting the applied overpotential, Ni can also be used as an efficient electrocatalyst in an acidic medium [53]. Even though Ni has sufficient electrocatalytic activity for hydrogen ion reduction, there is a great need for increasing its activity through alloying or increasing specific surface area through various structures [50–52, 54–57]. Ni possesses the best electrocatalytic activity among all nonprecious metals, and particularly its nanoparticles have a major impact on improving electrocatalytic activity [52, 58, 59].

This work is an attempt to design cheap and stable electrocatalysts for HER with reasonable activity to produce hydrogen. Silicon–carbon composite is used as a host material for metals, namely Ni and/or Pt, in small amounts to be used as hybrid electrocatalysts. The stability and catalytic activity of the as-prepared catalysts towards the HER in the acidic medium are the main targets of this study.

2 Experimental

2.1 Materials

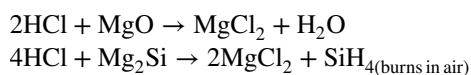
All the chemical materials used in this study are of analytical grade and were used as received without further purification. The used chemicals; Mg powder, carbon black (XC 72), H₂SO₄, HCl, HF, CH₃COOH, Polytetrafluoroethylene

(PTFE), $\text{Ni}(\text{NO}_3)_2 \cdot 6\text{H}_2\text{O}$, H_2PtCl_6 , ethylene glycol, and hydrazine were purchased from Fluka-Honeywell Research Chemicals. The crushed silica (SiO_2) is prepared by crushing the Sinai white sand with a ball mill for 8 h at a speed of 200 rpm to obtain particles with an average size of 100 nm. The double-distilled water with a resistivity of $17 \text{ M}\Omega \text{ cm}^{-1}$ was used for the preparation of various solutions.

2.2 Extraction of silicon from white sand

Si is extracted by mixing crushed SiO_2 and Mg powder with a molar ratio of 1:2, respectively, and blending them thoroughly using a stainless steel spatula. 100 g of the mixture was placed in a sealed stainless steel reactor and put in a programmed muffle furnace. The temperature was raised at a rate of $5 \text{ }^\circ\text{C min}^{-1}$ to the target temperature of $850 \text{ }^\circ\text{C}$. After the desired holding time (2 h), the furnace was switched off, and the sample was cooled slowly to room temperature within the furnace. Then, the reaction product cake was removed and crushed to a fine powder [60]. Recovery of Si from the reduction products was achieved by leaching the reduction products in three stages: (a) In the first stage, the powders were leached in 2 M HCl at $70 \text{ }^\circ\text{C}$ with continuous magnetic stirring to remove MgO and Mg_2Si ; (b) The second stage involved leaching the material with 2 M HCl and 25% acetic acid for the removal of Mg_2SiO_4 ; (c) To remove the remaining Mg_2SiO_4 , unreacted silica, and other contaminated metallic impurities, the material was further leached with 4.8% HF and 25% acetic acid at $70 \text{ }^\circ\text{C}$ in a polypropylene container for 1 h. Finally, all acids were removed by washing with warm demineralized water, and the product was filtered and dried.

From the economic and practical point of view, the filtrate produced in the first stage of leaching contains pure MgCl_2 :



So, the filtrate was evaporated under reduced pressure at $110 \text{ }^\circ\text{C}$ to obtain pure $\text{MgCl}_2 \cdot 6\text{H}_2\text{O}$ to be used for other purposes [61, 62].

2.3 Synthesis of C–Si, Ni/C–Si, Pt/C–Si, and Pt–Ni/C–Si catalysts

10 mg of carbon black was accurately weighed and heated for 1 h at $160 \text{ }^\circ\text{C}$ for activation. Then, definite amounts of silicon were added to prepare pastes with different wt% ratios of silicon:carbon composite. Each paste was synthesized by adding the appropriate weight of silicon to carbon, and 5 mL of methanol was added. The components were stirred well on the hot plate to ensure good mixing between carbon and

silicon. 1–2 drops of polytetrafluoroethylene (PTFE) were added to bind the components together to form a paste. Each paste was heated for 1 h at $160 \text{ }^\circ\text{C}$ for activation before each experiment.

The prepared electrodes were encapsulated in the form of a disc with an apparent circular surface area of 0.135 cm^2 . The best-chosen silicon–carbon powder, according to their mixing ratio, was modified with nickel and/or platinum metals. The silicon–carbon powder was mixed with a calculated amount of hydrated nickel nitrate $\text{Ni}(\text{NO}_3)_2 \cdot 6\text{H}_2\text{O}$ and dispersed in 20 mL of ethylene glycol with constant mechanical stirring on a hot plate for 3 h at $60 \text{ }^\circ\text{C}$ to intercalate the precursor ions into C–Si support pores. Then, the in-situ reduction of Ni^{2+} was achieved by adding the hydrazine dropwise to reduce Ni^{2+} into Ni^0 nanoparticles. After filtration and washing with acetone, the composite was collected and dried in an oven at $90 \text{ }^\circ\text{C}$ for 1 h. By applying the same procedures, the Pt/C–Si and Pt–Ni/C–Si hybrid materials were prepared using hexachloroplatinic acid H_2PtCl_6 as a platinum precursor.

2.4 Characterization procedures

The surface morphologies and chemical compositions of the prepared composites have been investigated using TEM, SEM, EDX, XPS, XRF, BET, and XRD. The TEM profile was investigated using the transmission electron microscope model Jeol jem 1400, Japan. The SEM images, elemental mapping, and EDX analysis were examined on a Zeiss Sigma 300 vp Field Emission electron microscope. X-ray Fluorescence analyzer, Malvern Panalytical, Epsilon 1, was used for the XRF analysis. An X-ray diffractometer, PANalytical model X, pert PRO, with a Cu K radiation ($k = 1.5418 \text{ \AA}$) and a scanning rate of 0.3 min^{-1} , was used for the XRD analysis. The X-ray photoelectron spectroscopy (XPS) data were collected on K-alpha (Thermo Fisher Scientific, USA) using monochromatic X-ray Al K-alpha radiation with a spot size of $400 \mu\text{m}$ at a pressure of 10^{-9} mbar and a full-spectrum pass energy of 200 eV and a narrow-spectrum pass energy of 50 eV. The textural analysis of the as-prepared composite catalytic systems was characterized by nitrogen adsorption–desorption isotherms at $196 \text{ }^\circ\text{C}$ using the NOVA 3200 apparatus, USA. For surface degassing, the samples were pretreated under vacuum (10^{-4} Torr) at $150 \text{ }^\circ\text{C}$

Table 1 The concentration of metallic species loaded onto the C–Si composite

Catalyst	Pt (%)	Ni (%)
10%Ni/[C–Si (1:1)]	–	9.65
10%Pt/[C–Si (1:1)]	9.82	–
7%Pt–3%Ni/[C–Si (1:1)]	6.85	2.57

for 2 h. From the adsorption isotherm branch, the surface areas (S_{BET}) were estimated using the BET equation. The pore size distribution was calculated from the isotherm's desorption branch using the Barrett, Joyner, and Halenda (BJH) method.

2.5 Electrochemical measurements

The electrochemical measurements towards the HER were carried out using C–Si, Ni/C–Si, Pt/C–Si, and Pt–Ni/C–Si catalysts as working electrodes in a three-electrode cell. The

reference electrode was a silver/silver chloride electrode (Ag/AgCl/sat. KCl solution), and the counter electrode was a Pt sheet. The electrochemical measurements were performed using linear sweep voltammetry (LSV), chronoamperometry, electrochemical impedance spectroscopy (EIS), and Tafel plots. The chronoamperometry measurements were recorded at -0.6 V, and the EIS measurements were recorded at the onset potential of HER according to each electrode within a frequency range from 10^5 to 10^2 Hz at an alternating current amplitude of 5 mV. All these electrochemical studies were performed using a potentiostat (CHI 660 Potentiostat/

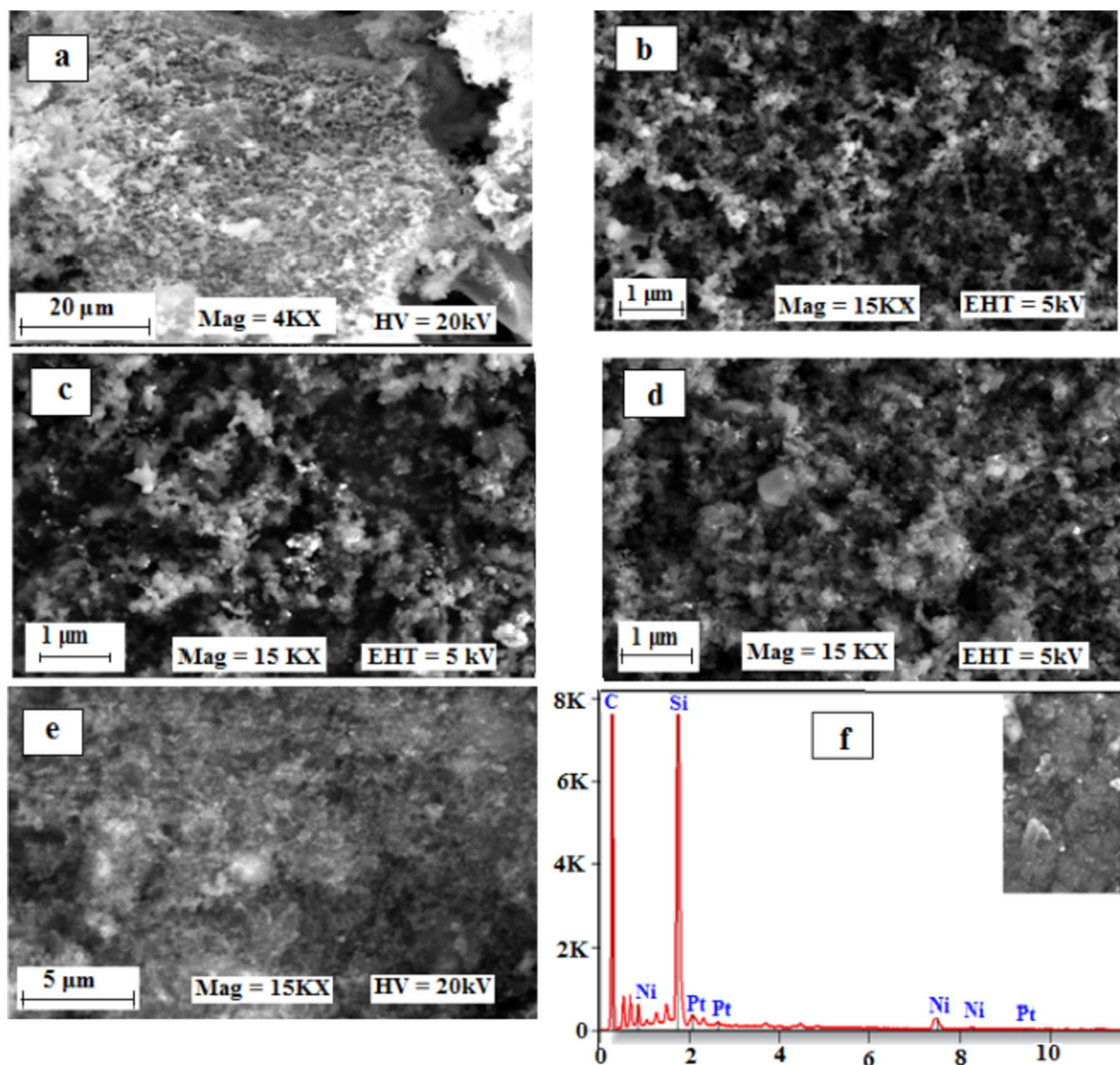


Fig. 1 SEM images of the samples **a** Si, **b** C–Si (1:1), **c** 10%Ni/[C–Si (1:1)], **d** 10%Pt/[C–Si (1:1)] and **e** [7%Pt–3%Ni]/[C–Si (1:1)]; and **f** EDX analysis of the composite [7%Pt–3%Ni]/[C–Si (1:1)]

Table 2 The values of weight% of the elements in the composite [7%Pt–3%Ni]/[C–Si (1:1)] obtained from EDX analysis

Element	Weight%
C	48.16
Si	41.37
Ni	3.75
Pt	6.62

Galvanostat). The measurements were carried out in a 0.5 M H₂SO₄ solution at a room temperature of 25 ± 0.2 °C.

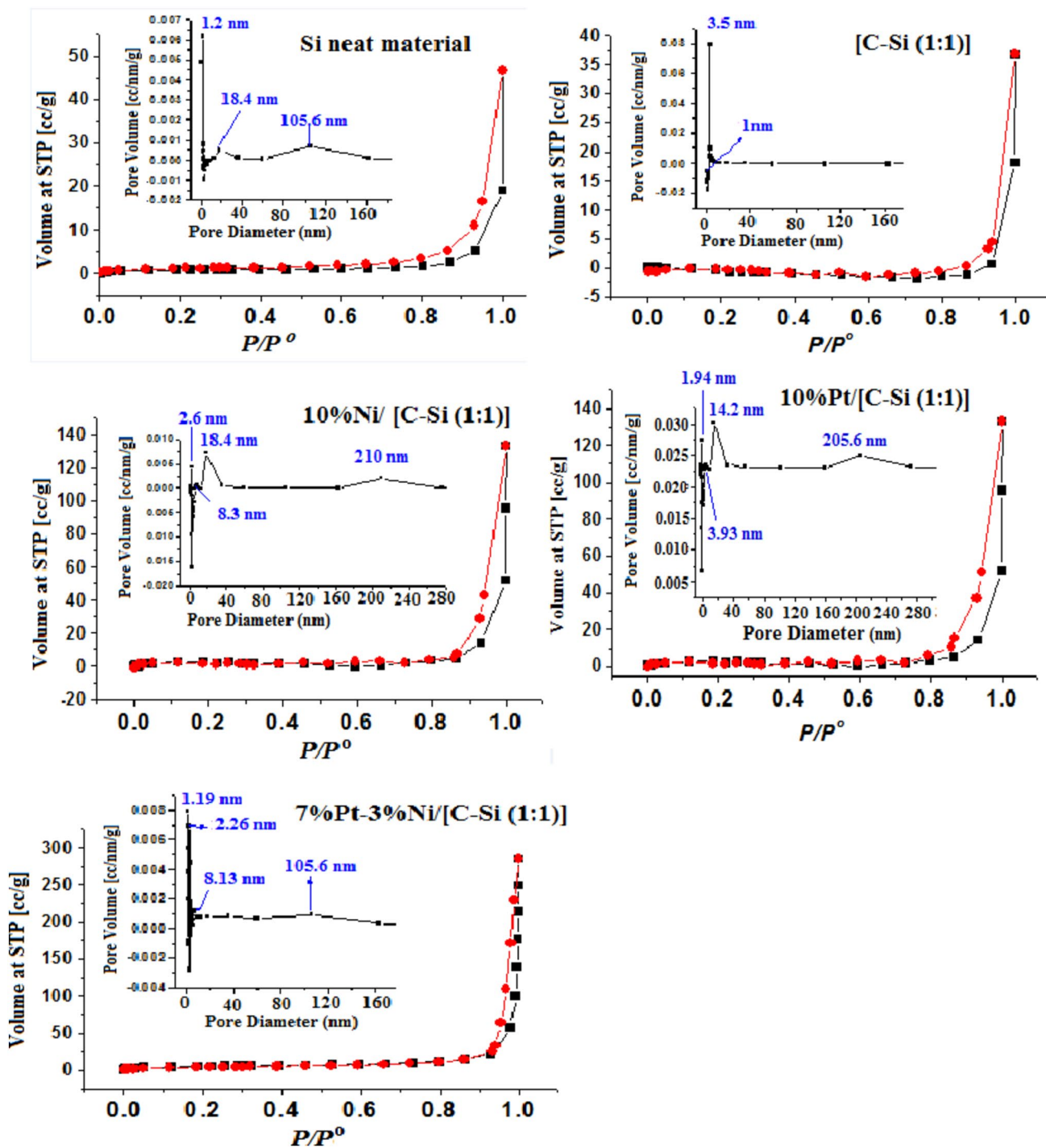


Fig. 2 The nitrogen adsorption–desorption isotherm and PSD of the as-prepared composites

3 Results and discussion

3.1 Constitutional investigation

To confirm the composition and the proportion of the metallic species of the as-prepared composite catalysts, 10%Ni/[C–Si (1:1)], 10%Pt/[C–Si (1:1)], and [7%Pt–3%Ni]/[C–Si (1:1)], the metallic elemental analysis was achieved via XRF analysis, Table 1. From the table the concentration of metallic species in each catalyst is very close to its weight during the preparation, which confirms the good accuracy of the preparation.

The scanning electron microscopy (SEM) images in Fig. 1a–e show the surface morphology of Si, C–Si (1:1), 10%Ni/[C–Si (1:1)], 10%Pt/[C–Si (1:1)], and [7%Pt–3%Ni]/[C–Si (1:1)], respectively. The surface morphology of Si (Fig. 1a) shows large agglomerates of white Si sheets with mesopores (cf. Table 3). The SEM image of C–Si (1:1) (Fig. 1b) exhibits a homogeneous distribution between carbon and silicon. On the other hand, the SEM image of 10%Ni/[C–Si (1:1)] (Fig. 1c) shows the same image of C–Si (1:1) but with lighted, homogeneously distributed dots that could indicate the presence of Ni particles on the surface. The SEM image of 10%Pt/[C–Si (1:1)] (Fig. 1d) is similar to the previous composite, but Pt is shown as grey-coloured dots and aggregates. Figure 1e represents the surface morphology of the composite [7%Pt–3%Ni]/[C–Si (1:1)], and it shows a very large homogeneity between the components of this composite. The elemental composition of this composite [7%Pt–3%Ni]/[C–Si (1:1)] is determined by the energy-dispersive X-ray (EDX) technique and is represented in Fig. 1f. Values of the wt% of the elements Si, C, O, Ni, and Pt for this composite are represented in Table 2. The relatively high percentage of C compared to Si (even though their ratio in the prepared composite is 1:1) is due to the small size of carbon, which in turn causes a higher distribution compared to Si.

Figure 2 shows the acquired N₂ adsorption–desorption isotherms across Si pristine material, [C–Si (1:1)], 10%Ni/[C–Si (1:1)], and [7%Pt–3%Ni]/[C–Si (1:1)]. All material isotherms belong most probably to type III according to the IUPAC classification, exhibiting an H3 hysteresis loop that suggests slit-like pores with capillary condensation in

heterogeneous micro- and/or mesopores (cf. the SEM and PSD profiles). Table 3 shows the surface parameters derived from adsorption–desorption isotherms, including specific surface areas (S_{BET} m² g^{−1}), pore volumes (V_p , cm³ g^{−1}), estimated at 0.95 p/p^0 , and average pore diameter (D_p^{cp}), assuming a cylindrical pore (cp) model derived from PSD curves depicted in Fig. 2. It is evident from the Table that adding C to the extracted Si may result in significant increases in surface area and pore size, where the hydraulic diameter is shifted from 1.2 nm for Si to 3.5 nm for [C–Si (1:1)], with the elimination of wider pores that are most probably filled with carbon. By loading the electrode surface with metallic species, a marked increase in surface area and pore volume, accompanied by a decrease in pore diameters, is observed. This may be related to the restructuring of the surface network.

XPS is a powerful analysis tool that is used to identify the surface chemical compositions and the oxidation states of the elements of the prepared composites. The XPS survey spectra of the as-prepared composite electrodes and their constituent metallic species are shown in Fig. 3. The presence of carbon, silicon, oxygen, nickel, and platinum are detected as the main peak elements in the prepared composite electrodes. The XP-spectra of Ni and Pt in the various composites display different peaks-relative intensities due to the difference in the environment and synergism between the metallic species [63–67]. The relative intensity of the peak characteristic for clean platinum, viz., Pt⁰, is higher in [7%Pt–3%Ni]/[C–Si (1:1)] than in 10%Pt/[C–Si (1:1)], which is consistent with the catalytic performance in which the Pt⁰ species provides the active sites for the oxidation reaction rather than Pt⁴⁺ [68]. Furthermore, the XP-spectra of Ni and Pt in the 10%Ni/[C–Si (1:1)] and 10%Pt/[C–Si (1:1)] differ markedly from the spectra in the [7%Pt–3%Ni]/[C–Si (1:1)], confirming Ni–Pt synergism.

XRD is another technique that is used to elucidate the phase analysis of the prepared composites. XRD analysis of [7%Pt–3%Ni]/[C:Si (1:1)] is represented in Fig. 4. It is noted in the figure that the characteristic peak of C has a very low intensity compared to Si, referring to the difference in the degree of crystallinity. The diffraction patterns illustrate well-defined diffraction peaks for Si according to the standard card (00-005-0565); peaks at 28.5°, 47.3°, 56.1°, 69.2°, and 76.3°; assigned to (111), (220), (311), (400),

Table 3 Surface characteristics of Si and various prepared catalytic composites

Item	Si-neat material	[C–Si (1:1)]	10%Ni/[C–Si (1:1)]	10%Pt / [C–Si (1:1)]	7%Pt–3%Ni/[C–Si (1:1)]
D_p^{CP} (nm)	31.419	142.72	45.604	41.40	29.356
$V_p^{0.95}$ (cm ³ g ^{−1})	0.0262	0.0239	0.071664	0.0946	0.1423
S_{BET} (m ² g ^{−1})	13.33	38.671	52.29	61.85	68.4

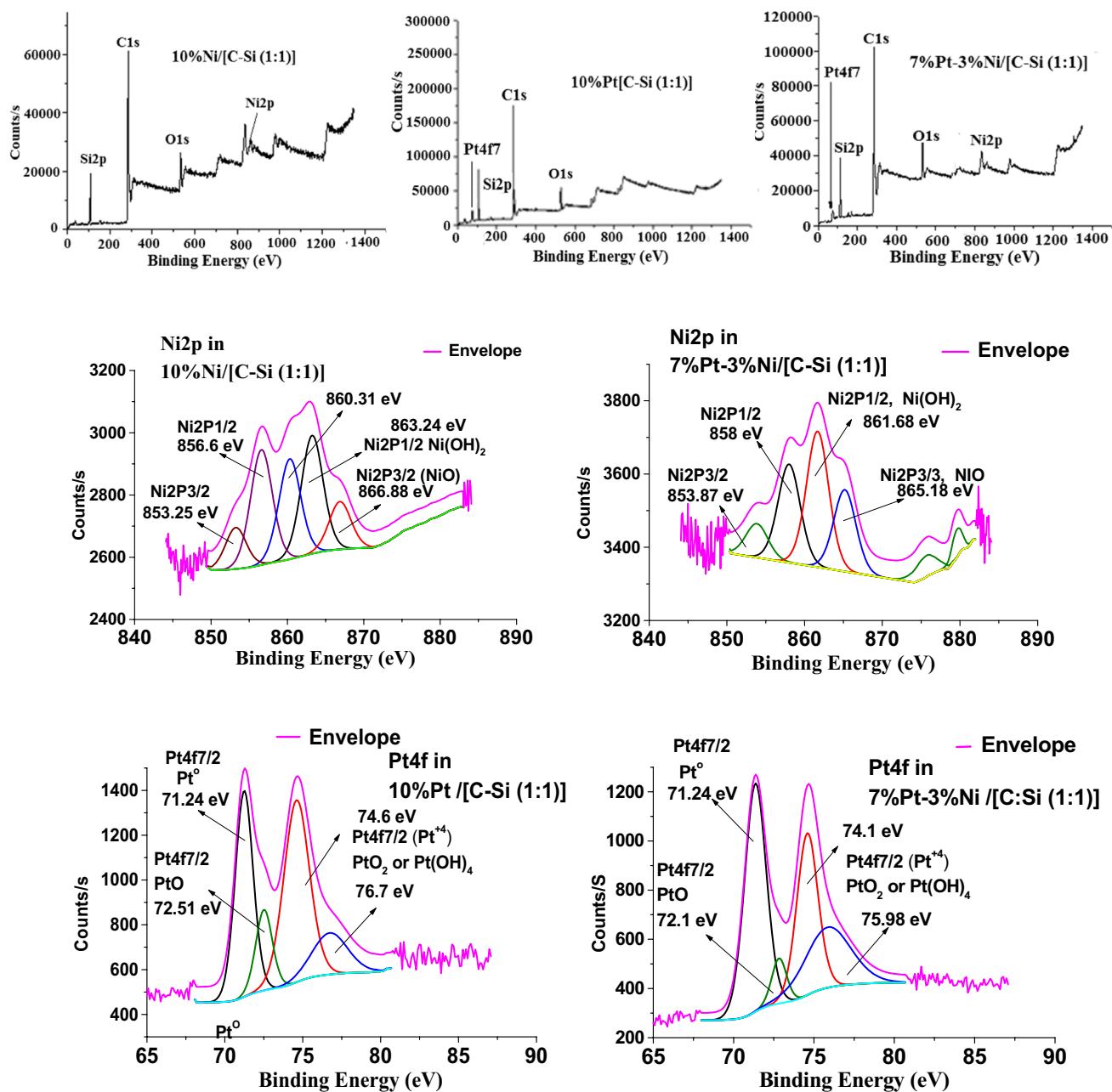


Fig. 3 XPS-spectrum of the as-prepared composite electrodes and their constituent metallic species

and (331) planes, respectively. A small, broad peak for C appeared at 25.5° , corresponding to the (002) plane according to the standard card (00-001-0640). The peaks assigned to Ni appear as a small broad peak at 43.1° and a small peak at 60.2° characteristic for (200) and (220), respectively, according to the standard card (00-001-1258). The peaks characteristic of Pt appear as a small broad peak at 39.6° , a peak at 47.1° , and a small peak at 68.3° assigned to (111), (200), and (220) planes, respectively, according to the standard card (01-085-5658).

3.2 Electrochemical properties and catalytic performance

Silicon has attracted much attention because of its novel physical and electrochemical properties [69]. Silicon in its pristine form has a high specific surface area, but it was found to have very little activity for the HER. So, modification of silicon was necessary to obtain a good catalyst towards HER. In this study, the bi-constitute composite material C–Si was first prepared and investigated in different ratios. In the second stage of the study,

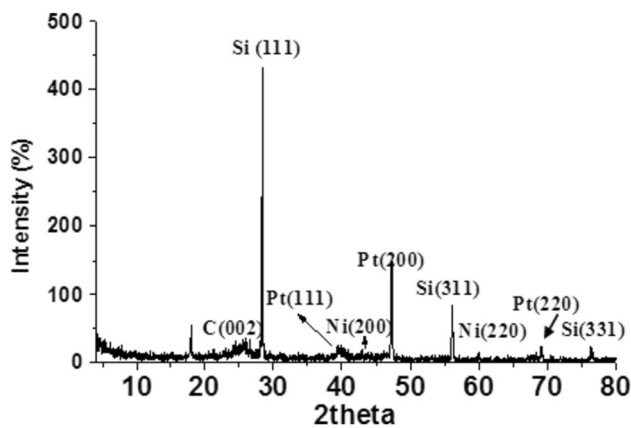


Fig. 4 XRD pattern of the composite [7%Pt-3%Ni]/[C-Si (1:1)]

tri- and tetra-constitute composites of Ni/C-Si, Pt/C-Si, and Pt-Ni/C-Si were prepared and optimized.

Firstly, carbon powder was mixed with silicon in various weight ratios to increase the specific surface area of the prepared electrodes and optimize the best ratio for obtaining good catalytic performance. The electrocatalytic activity of the prepared composites towards HER was studied using the LSV technique at 25 °C in the potential range from +0.1 to -1.3 V (Ag/AgCl) at a scan rate of 5 mV s⁻¹ in 0.5 M H₂SO₄, as shown in supplementary Fig. s1. This study showed that, carbon enhances the activity of silicon, and the composite C:Si with a ratio of 50%:50% gives the best results compared to the other ratios either with respect to the value of the onset potential of this reaction or the rate of HER. This ratio gives the least negative onset hydrogen evolution potential (-0.741 V) and the highest rate of HER (45.49 μA cm⁻² s⁻¹) compared to other C:Si ratios in this study. The rate value of hydrogen evolution was deduced from the slope of the straight segment of the cathodic current of hydrogen evolution (mA cm⁻² V⁻¹) multiplied by the scan rate [5 mV s⁻¹].

For all the foregoing studies, a carbon-silicon mixture with a ratio of 50%:50% was chosen as the host composite material for supporting the metal particles. Nickel metal was incorporated into the silicon-carbon matrix via the in-situ reduction of Ni precursor to obtain Ni/(C-Si) composites. Various electrodes were prepared by loading different weight ratios of Ni onto C:Si (1:1), and their activity towards the HER was studied in the potential range from +0.1 to -1.0 V (Ag/AgCl) at a scan rate of 5 mV s⁻¹. The electrochemical behaviour of the prepared nickel-modified composites is represented in supplementary Fig. s2. It is noticed that the composite with a ratio of 10% Ni and 90% [C:Si (1:1)] shows the highest rate of HER (170.2 μA cm⁻² s⁻¹), the least onset hydrogen evolution potential (-0.288 V), and the lowest overpotential [0.671 V vs. (Ag/AgCl)] at 10 mA cm⁻² compared to other ratios.

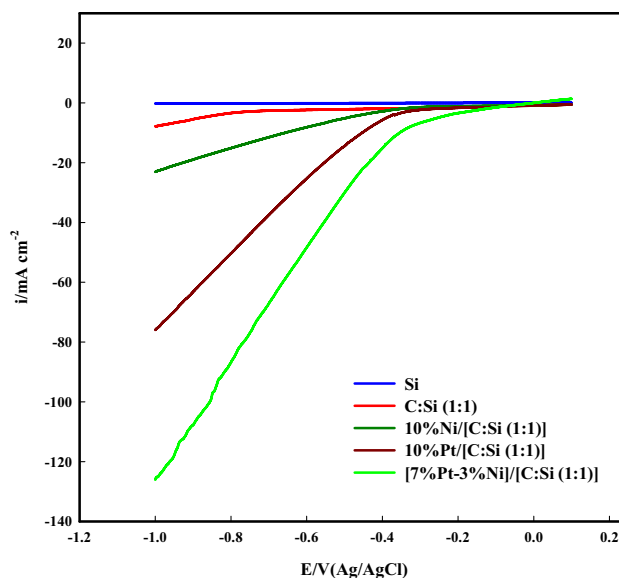


Fig. 5 LSV of the prepared composites Si, C-Si (1:1), 10%Ni/[C-Si (1:1)], 10%Pt/[C-Si (1:1)] and [7%Pt-3%Ni]/[C-Si (1:1)] in 0.5 M H₂SO₄ at 5 mV s⁻¹

Despite the initial high electrochemical activity of nickel, it may be deactivated during operation due to hydrogen adsorption, promoted by the strong Ni-H_{ad} bond strength, causing the shielding of Ni-surface active sites. Also, this results in performance degradation with an increase in the overpotential under constant current stress [70–72]. So, adding another active metal with nickel would solve this problem by increasing the activity and stability towards the HER. Platinum is considered the best catalyst for HER [73, 74], as it exhibits high current density and nearly zero HER overpotential [47]. However, platinum is also livery expensive, and therefore, its amount should be reduced as much as possible to reduce the cost. So, platinum is prepared in a composite with a ratio of 10% Pt and 90% [C:Si (1:1)] for comparison with Ni composite, and this amount is reduced during the modification with Ni metal in the composite.

HER was investigated using the following prepared electrodes; Si, C-Si (1:1), 10%Ni/[C-Si (1:1)], 10%Pt/[C-Si (1:1)], and [7%Pt-3%Ni]/[C-Si (1:1)] (optimized ratio) in 0.5 M H₂SO₄ solution in the potential range from +0.1 to -1.0 V (Ag/AgCl) at a scan rate of 5 mV s⁻¹ as shown in Fig. 5. It is observed that the electrode [7%Pt-3%Ni]/[C-Si (1:1)] gives the best result compared to other prepared electrodes [highest HER rate (940.95 μA cm⁻² s⁻¹), lowest overpotential [0.358 V vs. (Ag/AgCl) ≈ 0.161 V vs. (RHE)] at 10 mA cm⁻². This means that the incorporation of a small amount of platinum and nickel metals into the carbon-silicon composite enhanced their activity towards the HER. This may be linked with the synergetic effects

Table 4 The onset potential, overpotential at 10 mA cm⁻² and the rate of HER (μA cm⁻² V⁻¹) vs. (Ag/AgCl) of the Si-neat material and the prepared composites

Composite	Onset potential of H ₂ evolution (V) vs. (Ag/AgCl)	Overpotential of H ₂ evolution (V) vs. (Ag/AgCl) at 10 mA cm ⁻²	Rate of HER (μA cm ⁻² s ⁻¹) vs. (Ag/AgCl)
Si	- 1.000	More negative than 1.000	5.00 × 10 ⁻⁴
C-Si (1:1)	- 0.741	More negative than 1.000	45.485
10%Ni/[C-Si (1:1)]	- 0.288	0.671	170.22
10Pt/[C-Si (1:1)]	- 0.259	0.455	595.25
[7%Pt-3%Ni]/[C-Si (1:1)]	- 0.215	0.358	940.95

Table 5 Values of current density (mA cm⁻²), mass activity (mA g⁻¹), current per active surface area (mA cm⁻²), and turn over frequency (s⁻¹) for the prepared composites at - 0.6 V (Ag/AgCl)

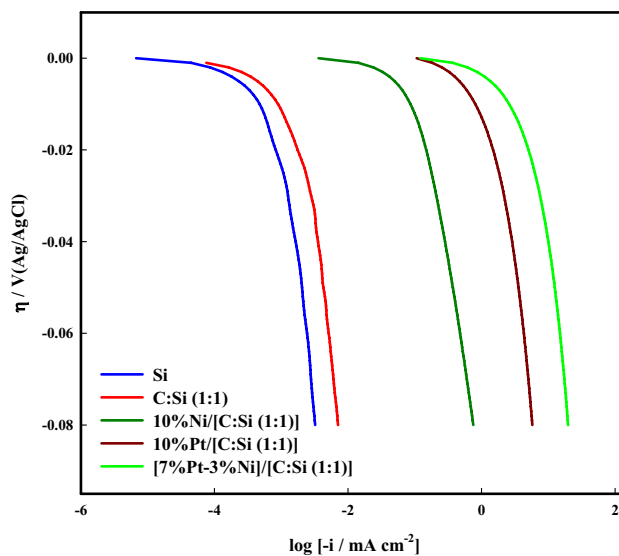
Composite	Current density (mA cm ⁻²)	Current density (mA g ⁻¹) for 10 mg mass electrode	Current density per active surface area (mA cm ⁻²)	Turn over frequency (s ⁻¹)
Si	0.296	3.996	—	—
C:Si (1-1)	1.751	23.64	—	—
10%Ni/[C-Si (1:1)]	7.675	103.6	2.800	3.273 × 10 ⁻⁴
10%Pt/[C-Si (1:1)]	25.41	343.0	1.769	3.534 × 10 ⁻³
[7%Pt-3%Ni]/[C-Si (1:1)]	47.59	642.5	3.125	4.219 × 10 ⁻³

of the binary metallic species in the prepared composites, as discussed in the XPS analysis, and the intrinsic activity of platinum [50, 75, 76]. The values of hydrogen evolution onset potential, overpotential at 10 mA cm⁻² and the rate of HER (μA cm⁻² s⁻¹) are shown in Table 4. The rate values were calculated from the slopes of the straight line relations represented in Fig. s3. These lines are obtained by plotting a relation between potential values, selected from the straight segments of hydrogen evolution in Fig. 5 at potential values from - 1.0 V till - 0.4 V, and their corresponding current density values.

The enhanced catalysis of the prepared composites as shown in Table 4 may be due to the increase in the electroactive surface area. So, the active surface area of the prepared composites was evaluated by recording the CV response of 1.0 mM [Fe(CN)₆]^{3-/4-} (1:1) in 0.1 mol L⁻¹ KCl solution at different scan rates as shown in Fig. s4. The surface area is calculated using the Randles-Sevcik equation [77]:

$$I_p = (2.69 \times 10^5) n^{3/2} A D^{1/2} C \nu^{1/2},$$

where I_p is the peak current (A), n is the number of the transferred electrons in the electrochemical process ($n = 1$), A is the electrode surface area (cm²), D is the diffusion coefficient (6.5×10^{-6} cm² s⁻¹ [77]), C is the concentration of the redox probe (mol cm⁻³), and ν is the applied scan rate (V/s). By substituting the slope of I_p versus $\nu^{1/2}$ (see Fig. s4) in the above equation, the electroactive surface area was

**Fig. 6** Tafel plot of the prepared composites Si, C-Si (1:1), 10%Ni/[C-Si (1:1)], 10%Pt/[C-Si (1:1)] and [7%Pt-3%Ni]/[C-Si (1:1)] in 0.5 M H₂SO₄ at 1 mV s⁻¹

calculated to be 0.370, 1.939, and 2.056 for 10%Ni/[C-Si (1:1)], 10%Pt/[C-Si (1:1)], and [7%Pt-3%Ni]/[C-Si (1:1)], respectively.

Another activity metric used as a reaction kinetics indicator is turnover frequency (TOF). It shows the amount of hydrogen that evolves each unit of time at a single catalytically active site [78]. The following equation [79]

can be used to get TOF for the hydrogen evolution reaction under the assumption that Faradic efficiency is 100%:

$$\text{TOF} = I/2 \times F \times m,$$

where I is the current (A), 2 is the number of electrons needed to produce a molecule of the product H_2 , F is the Faraday constant ($96,500 \text{ C mol}^{-1}$), m is the number of moles of metallic active species in the composite. The number of moles of metallic species is calculated according to the mass values obtained from XRF analysis, and each composite mass was 10 mg. Then, the number of moles of metallic species in 10%Ni/[C–Si (1:1)], 10%Pt/[C–Si (1:1)], and [7%Pt–3%Ni]/[C–Si (1:1)] are 1.64×10^{-5} , 5.03×10^{-6} , and 7.89×10^{-6} mol. A comparison between current density (mA cm^{-2}), mass activity (mA g^{-1}), current per active surface area (mA cm^{-2}), and turn over frequency (s^{-1}) for the prepared composites Si, C–Si (1:1), 10%Ni/[C–Si (1:1)], 10%Pt/[C–Si (1:1)], and [7%Pt–3%Ni]/[C–Si (1:1)] is tabulated in Table 5. It is observed that all

the current density values are increased with the sequence; $\text{Si} < \text{C–Si (1:1)} < 10\% \text{Ni}/[\text{C–Si (1:1)}] < 10\% \text{Pt}/[\text{C–Si (1:1)}] < [7\% \text{Pt–3\%Ni}]/[\text{C–Si (1:1)}]$ except the current density per active surface area. The lower value for 10%Pt/[C–Si (1:1)] compared to 10%Ni/[C–Si (1:1)] may be due to the large size of Pt compared to Ni of the same ratio. The values obtained in case of [7%Pt–3%Ni]/[C–Si (1:1)] may be due to the synergism between Pt and Ni in the prepared composite.

Tafel plot represents the relation between the polarization current density and the overpotential as a probe of the intrinsic behaviour of the electrocatalysts according to the following equation [48, 80]:

$$\eta = a + b \log(-i),$$

where “ η ” is the overpotential (V), “ a ” represents the intercept, “ b ” represents the Tafel slope, and “ i ” represents the cathodic current density. The exchange current density (i_o) is an important parameter for the HER, and it can be calculated from the relation: $\log i_o = (-b/a)$. The high value of i_o represents the better electrocatalyst towards the HER. Figure 6 represents the Tafel plots for Si and the composites C–Si (1:1), 10%Ni/[C–Si (1:1)], 10%Pt/[C–Si (1:1)], and [7%Pt–3%Ni]/[C–Si (1:1)] in 0.5 M H_2SO_4 solution at a scan rate of 1 mV s^{-1} . It is observed that all the prepared composites have nearly the same slope, which indicates that the mechanism of hydrogen evolution is the same. The slope and exchange current density values of the prepared composites are represented in Table 6. From these results, it is indicated that the prepared composite [7%Pt–3%Ni]/[C–Si (1:1)] is the best one towards the HER compared to other prepared composites. A comparison between our work and other work in literature is represented in Table 7.

Table 6 Tafel slope (b), and exchange current density (i_o) for the Si-neat material, the prepared composites C–Si (1:1), 10%Ni/[C–Si (1:1)], 10%Pt/[C–Si (1:1)] and [7%Pt–3%Ni]/[C–Si (1:1)] in 0.5 M H_2SO_4

Composite	Tafel slope (b) [V dec ⁻¹]	Exchange current density (i_o) [mA cm ⁻²]
Si	0.141	0.00088
C:Si (1–1)	0.135	0.00185
10%Ni/[C–Si (1:1)]	0.095	0.11018
10%Pt/[C–Si (1:1)]	0.133	1.48913
[7%Pt–3%Ni]/[C–Si (1:1)]	0.136	5.34491

Table 7 Comparison between our study and other similar studies in literature

Catalyst	Electrolyte	Overpotential for HER (mV) vs. (RHE) at 10 mA cm^{-2}	Tafel slope (mV dec ⁻¹)	References
[7%Pt–3%Ni]/[C–Si (1:1)]	0.5 M H_2SO_4	161	136	This work
Pt–Ag/SiNW	0.5 M H_2SO_4	135	70	[25]
Re–SiNW	0.5 M H_2SO_4	390	81	[81]
WS2/nano–Si etched	0.5 M H_2SO_4	140	45	[82]
Copper–silica	0.5 M H_2SO_4	200	67	[83]
Mesoporous 95% Ni/Pt	0.5 M H_2SO_4	140	63	[84]
PtM/p–GO	0.5 M H_2SO_4	18	23	[85]
Pt/NC–850	0.5 M H_2SO_4	17	32	[86]
Ni-doped CoP/Co2P NSs	0.5 M H_2SO_4	100	66	[87]
Graphene-based Ni–Pt coated electrode	1 M KOH	268	139.1	[50]
Pt–Ni (1:1)/rGO	0.1 M KOH	147	72	[88]
Pt2@Ni–rGO	1 M KOH	200	328	[89]
Ni–Fe–Pt	1 M KOH	463	81	[90]

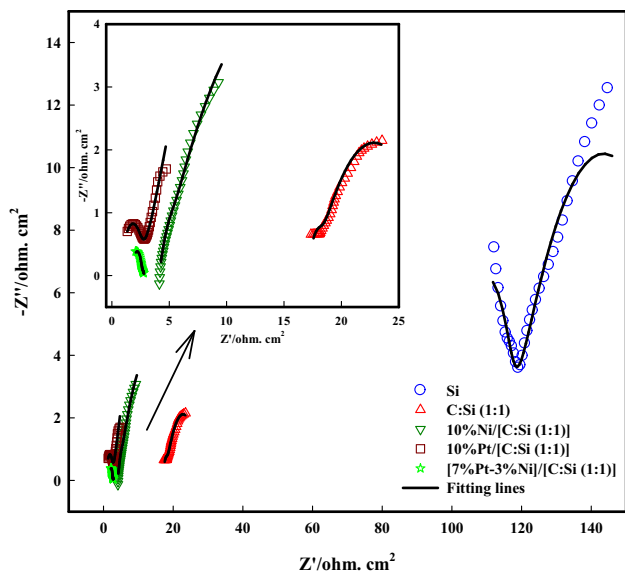


Fig. 7 Nyquist plot of the Si-neat material and the prepared composites C–Si (1:1), 10%Ni/[C–Si (1:1)], 10%Pt/[C–Si (1:1)] and [7%Pt–3%Ni]/[C–Si (1:1)] at HER onset potential of each composite. The inset figure represents magnification of Nyquist plot of the prepared composites C–Si (1:1), 10%Ni/[C–Si (1:1)], 10%Pt/[C–Si (1:1)] and [7%Pt–3%Ni]/[C–Si (1:1)]

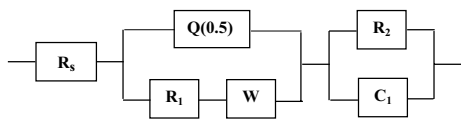


Fig. 8 Equivalent circuit used for fitting the Nyquist plot

Electrochemical impedance spectroscopy (EIS) was used to evaluate the electrode polarization and understand the charge transfer kinetics towards the HER. The observed EIS spectra from these measurements at lower frequencies indicate the material behaviour, and at a higher frequency, they are usually associated with the bulk electrolyte behaviour [25]. EIS measurements were recorded at the onset potential of each electrode within a frequency range from 10^5 to 10^2 Hz at an alternating current amplitude of 5 mV.

Table 8 The fitting parameters for the Si-neat material and the prepared composites as calculated by the instrument software for the electrode with area 0.135 cm^2

Item	R_s [Ω]	$Q_{(0.5)}$ [F]	R_1 [Ω]	W [Ω]	R_2 [Ω]	C_1 [F]
Si	746	8.135×10^{-5}	426.3	4.625×10^8	97.01	1.534×10^{-8}
C–Si (1:1)	126.5	4.295×10^{-4}	75.5	2.616×10^4	5.017	6.675×10^{-7}
10%Ni/[C–Si (1:1)]	30.14	6.784×10^{-4}	156.1	6.325×10^2	2.606	1.222×10^{-5}
10Pt/[C–Si (1:1)]	3.305	1.371×10^{-4}	11.95	1.755×10^{-3}	6.537	6.395×10^{-7}
[7%Pt–3%Ni]/[C–Si (1:1)]	13.29	2.337×10^{-3}	2.657	1.496×10^4	4.994	5.254×10^{-7}

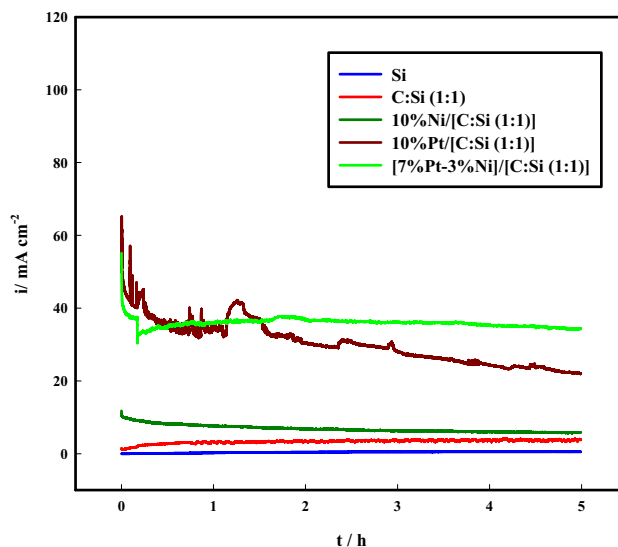


Fig. 9 $I-t$ curves of the Si-neat material and the prepared composites [C–Si (1:1)], 10%Ni/[C–Si (1:1)], 10%Pt/[C–Si (1:1)] and [7%Pt–3%Ni]/[C–Si (1:1)] at -0.6 V (Ag/AgCl) in $0.5 \text{ M H}_2\text{SO}_4$

Bode plots of the prepared composites are shown in Fig. s5. The impedance (Z) of HER decreases in the order $\text{Si} > \text{C–Si (1:1)} > 10\% \text{Ni}/[\text{C–Si (1:1)}] > 10\% \text{Pt}/[\text{C–Si (1:1)}] > [7\% \text{Pt–3\%Ni}]/[\text{C–Si (1:1)}]$. The lowest value of (Z) indicates the high conductivity and catalytic activity towards the charge transfer reaction of the HER, which confirms that the composite [7%Pt–3%Ni]/[C–Si (1:1)] is the best catalyst towards the HER among the employed electrodes. The Nyquist plot for the prepared composites is constructed and represented in Fig. 7. The capacitive semicircle diameters decrease with the insertion of carbon and Pt–Ni metal particles till reaching the best behaviour for the composite [7%Pt–3%Ni]/[C–Si (1:1)]. Magnification Nyquist plot of the prepared composites C–Si (1:1), 10%Ni/[C–Si (1:1)], 10%Pt/[C–Si (1:1)] and [7%Pt–3%Ni]/[C–Si (1:1)] is represented in inset Fig. 7.

The fitting data were applied for these composites, and the equivalent circuit that is used for fitting is represented in Fig. 8. The equivalent circuit was found to compose of

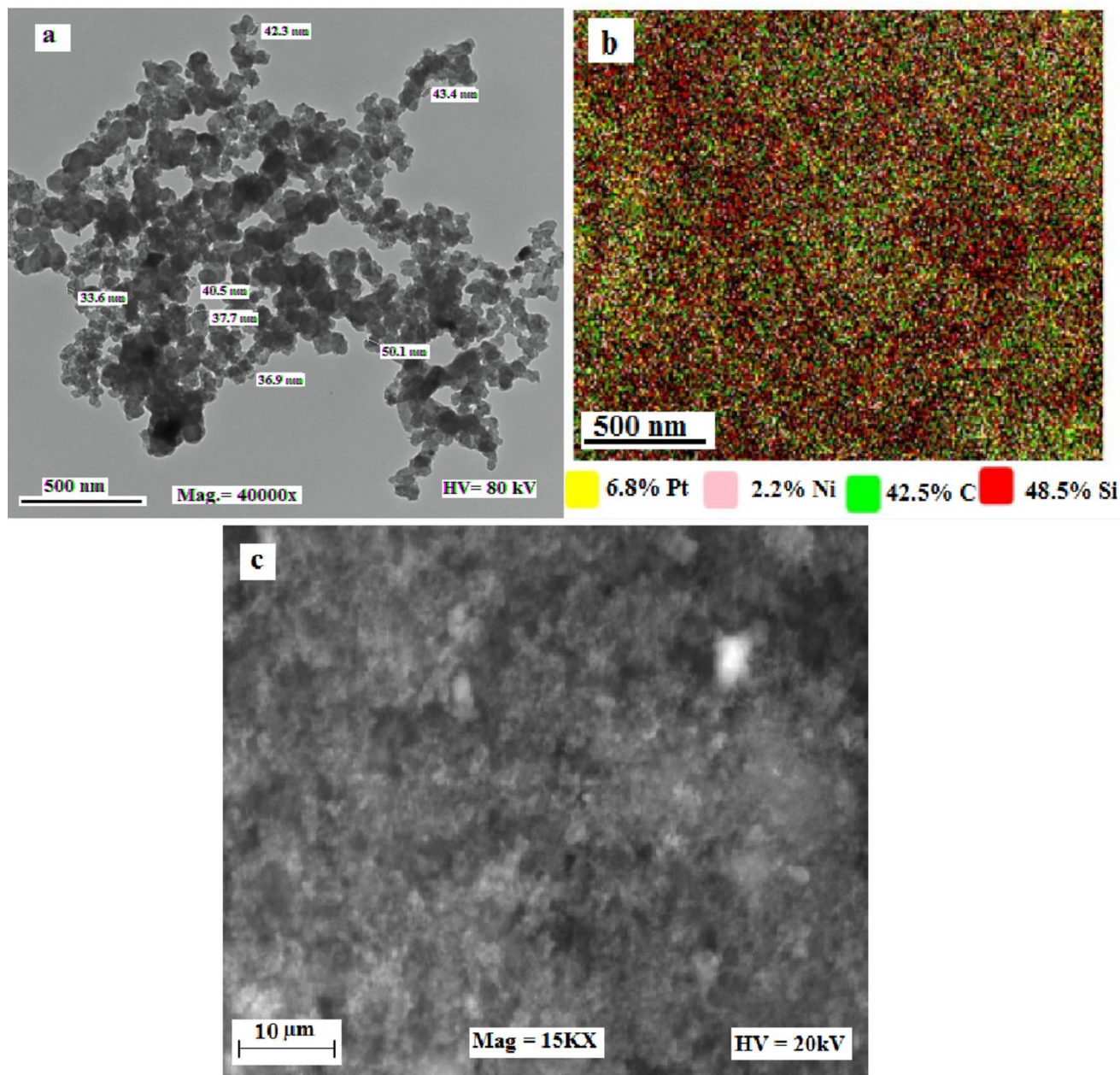


Fig. 10 **a** TEM, **b** elemental mapping, and **c** SEM image of [7%Pt–3%Ni]/[C–Si (1:1)] exploited catalyst

solution resistance (R_s), constant phase element [$Q(0.5)$], charge transfer resistance (R_1), Warburg diffusion component (W), surface adsorption capacitance (C_1), and surface adsorption resistance (R_2) [25, 91, 92]. All fitting parameters for the prepared composites as calculated by the instrument software are represented in Table 8. All parameters are tabulated as taken from the device without being multiplied by surface area. The presence of Warburg impedance in the circuit confirms that mass transport is limited by the surface protective film. The presence of a constant phase

element confirms the porosity of the prepared composites. In comparison to other materials, the composite 7%Pt–3%Ni/[C–Si (1:1)] delivers the lowest values of the charge transfer resistance which supports the electrode's maximum activity towards the HER.

3.3 Durability test

The stability of the prepared catalysts is an essential parameter for the practical application of the synthesized

electrocatalysts. It is measured by the variation in current versus time ($I-t$ curve), where the catalyst with excellent stability shows a negligible loss in current density with time. $I-t$ curves of the Si-neat material and the prepared composites: C–Si (1:1), 10%Ni/[C–Si (1:1)], 10%Pt/[C–Si (1:1)] and [7%Pt–3%Ni]/[C–Si (1:1)] at -0.6 V (Ag/AgCl) in 0.5 M H_2SO_4 for 5 h are represented in Fig. 9. It is observed that the stability of the prepared composites can be arranged in the following order: Si < C–Si (1:1) < 10%Ni/[C–Si (1:1)] < 10%Pt/[C–Si (1:1)] < [7%Pt–3%Ni]/[C–Si (1:1)], as indicated from the cathodic current density values obtained for these composites. The current density in case of 10%Pt/[C–Si (1:1)] composite decreases rapidly from the start current density and reaches 22.35 mA cm^{-2} after 5 h compared to that at [7%Pt–3%Ni]/[C–Si (1:1)] which attains stability early and reaches 34.28 mA cm^{-2} after 5 h. This means that the presence of Pt and Ni in the composite add extra stability to the catalyst towards HER compared to the presence of Pt only in the composite. To confirm the stability of [7%Pt–3%Ni]/[C–Si (1:1)] as a promised catalyst, the exploited catalyst was investigated by TEM, SEM, and elemental mapping as shown in Fig. 10. The figure exhibits the homogeneity of the composite catalyst and its stability during the catalytic HER.

4 Conclusion

The study shows that the Si-neat material has very low activity towards HER. However, doping with C, Ni, and Pt significantly enhances the electrocatalytic activity by increasing the composite electrode surface area and the synergism between the constitutional species. Ni/C–Si composite electrode exhibits deactivation during the HER process. The incorporation of Pt in a small ratio with Ni into [C–Si (1:1)] enhances the stability and activity of the electrode via the synergism between Ni–Pt bimetallic species. All the tests done for the as-prepared composite electrodes show that [7%Pt–3%Ni]/[C–Si (1:1)] has the best activity and stability towards the HER in acidic medium compared to other prepared composites in this study. It shows the lowest overpotential [0.358 V vs. (Ag/AgCl) ≈ 0.161 V vs. (RHE)] at 10 mA cm^{-2} , best exchange current density (5.345 mA cm^{-2}), and the lowest charge transfer resistance (2.657 Ω). It gives the highest turn over frequency (TOF) value of 4.219×10^{-3} s $^{-1}$, and 642 mA g^{-1} for mass activity compared to other prepared composites. In addition, it shows good stability towards the hydrogen evolution reaction as the current density reaches about 34.28 mA cm^{-2} after 5 h. Therefore, this work represents a promising approach for designing and fabricating electrocatalysts with improved

electric energy for the production of green hydrogen to improve energy conversion efficiency.

Supplementary Information The online version contains supplementary material available at <https://doi.org/10.1007/s10800-023-01988-8>.

Author contributions MNE: methodology; resources; software; validation; visualization; roles/writing—original draft. MAAR: conceptualization; data curation; formal analysis; resources; supervision; validation; visualization; writing—review & editing. NHS: conceptualization; data curation; formal analysis; investigation; methodology; resources; software; validation; visualization; roles/writing—original draft. MAS: conceptualization; data curation; formal analysis; methodology; resources; supervision; validation; visualization; writing—review & editing.

Funding Open access funding provided by The Science, Technology & Innovation Funding Authority (STDF) in cooperation with The Egyptian Knowledge Bank (EKB).

Declarations

Conflict of interest There are no conflicts to declare.

Open Access This article is licensed under a Creative Commons Attribution 4.0 International License, which permits use, sharing, adaptation, distribution and reproduction in any medium or format, as long as you give appropriate credit to the original author(s) and the source, provide a link to the Creative Commons licence, and indicate if changes were made. The images or other third party material in this article are included in the article's Creative Commons licence, unless indicated otherwise in a credit line to the material. If material is not included in the article's Creative Commons licence and your intended use is not permitted by statutory regulation or exceeds the permitted use, you will need to obtain permission directly from the copyright holder. To view a copy of this licence, visit <http://creativecommons.org/licenses/by/4.0/>.

References

- Potocnik J (2007) Renewable energy sources and the realities of setting an energy agenda. *Science* 315:810–811
- Ray U, Sarkar S, Banerjee D (2022) Silicon nanowires as an efficient material for hydrogen evolution through catalysis: a review. *Catal Today*. <https://doi.org/10.1016/j.cattod.2022.11.025>
- Chow J, Kopp RJ, Portney PR (2003) Energy resources and global development. *Science* 302:1528–1531. <https://doi.org/10.1126/science.1091939>
- Uyar TS, Beşikci D (2017) Integration of hydrogen energy systems into renewable energy systems for better design of 100% renewable energy communities. *Int J Hydrogen Energy* 42:2453–2456. <https://doi.org/10.1016/j.ijhydene.2016.09.086>
- Wang J, Xu F, Jin H et al (2017) Non-noble metal-based carbon composites in hydrogen evolution reaction: fundamentals to applications. *Adv Mater*. <https://doi.org/10.1002/adma.201605838>
- Schalenbach M, Tjarks G, Carmo M et al (2016) Acidic or alkaline? Towards a new perspective on the efficiency of water electrolysis. *J Electrochem Soc* 163:F3197–F3208. <https://doi.org/10.1149/2.0271611jes>
- Hosseini SE, Wahid MA (2016) Hydrogen production from renewable and sustainable energy resources: promising green

- energy carrier for clean development. *Renew Sustain Energy Rev* 57:850–866. <https://doi.org/10.1016/j.rser.2015.12.112>
8. Yang L, Zhou W, Hou D et al (2015) Porous metallic MoO₂-supported MoS₂ nanosheets for enhanced electrocatalytic activity in the hydrogen evolution reaction. *Nanoscale* 7:5203–5208. <https://doi.org/10.1039/c4nr06754a>
 9. Armaroli N, Balzani V (2011) The hydrogen issue. *ChemSusChem* 4:21–36. <https://doi.org/10.1002/cssc.201000182>
 10. Zhou W, Chen S, Meng X et al (2023) Energy-saving cathodic H₂ production enabled by non-oxygen evolution anodic reactions: a critical review on fundamental principles and applications. *Int J Hydrogen Energy*. <https://doi.org/10.1016/j.ijhydene.2023.01.063>
 11. Yu X, Gao B, Feng B et al (2023) Modular electrochemical production of hydrogen using Mott–Schottky Co₉S₈/Ni₃S₂ heterojunction as a redox mediator. *Int J Hydrogen Energy* 48:16184–16197
 12. Li X, Liu Y, Wu Y et al (2021) Vanadium doped nickel cobalt phosphide as an efficient and stable electrode catalyst for hydrogen evolution reaction. *J Electroanal Chem* 902:115812
 13. Abdel Hamid Z, Hassan HB, Sultan M (2020) Electrodeposition of Ni–W and Ni–W–P films using a pulse current technique and their application for hydrogen evolution in an acidic solution. *Anti-Corros Methods Mater* 67:38–47. <https://doi.org/10.1108/ACMM-09-2019-2176>
 14. Yin H, Zhao S, Zhao K et al (2015) Ultrathin platinum nanowires grown on single-layered nickel hydroxide with high hydrogen evolution activity. *Nat Commun* 6:1–8. <https://doi.org/10.1038/ncomms7430>
 15. Gao MR, Liang JX, Zheng YR et al (2015) An efficient molybdenum disulfide/cobalt diselenide hybrid catalyst for electrochemical hydrogen generation. *Nat Commun*. <https://doi.org/10.1038/ncomms6982>
 16. Zheng Y, Jiao Y, Zhu Y et al (2014) Hydrogen evolution by a metal-free electrocatalyst. *Nat Commun* 5:2–9. <https://doi.org/10.1038/ncomms4783>
 17. Fei H, Dong J, Arellano-Jiménez MJ et al (2015) Atomic cobalt on nitrogen-doped graphene for hydrogen generation. *Nat Commun* 6:1–8. <https://doi.org/10.1038/ncomms9668>
 18. Liu Q, He YM, Weng X et al (2018) One-pot aqueous fabrication of reduced graphene oxide supported porous PtAg alloy nanoflowers to greatly boost catalytic performances for oxygen reduction and hydrogen evolution. *J Colloid Interface Sci* 513:455–463. <https://doi.org/10.1016/j.jcis.2017.11.026>
 19. Liu M, Yang L, Liu T et al (2017) Fe₂P/reduced graphene oxide/Fe₂P sandwich-structured nanowall arrays: a high-performance non-noble-metal electrocatalyst for hydrogen evolution. *J Mater Chem A* 5:8608–8615. <https://doi.org/10.1039/c7ta01791j>
 20. Milazzo RG, Privitera SMS, Scalese S, Lombardo SA (2019) Effect of morphology and mechanical stability of nanometric platinum layer on nickel foam for hydrogen evolution reaction. *Energies*. <https://doi.org/10.3390/en12163116>
 21. Helm ML, Stewart MP, Bullock RM et al (2011) A synthetic nickel electrocatalyst with a turnover frequency above 100,000 s⁻¹ for H₂ production. *Science* 333:863–866. <https://doi.org/10.1126/science.1205864>
 22. Jaramillo TF, Jørgensen KP, Bonde J et al (2007) Identification of active edge sites for electrochemical H₂ evolution from MoS₂ nanocatalysts. *Science* 317:100–102. <https://doi.org/10.1126/science.1141483>
 23. Morales-Guio CG, Stern LA, Hu X (2014) Nanostructured hydro-treating catalysts for electrochemical hydrogen evolution. *Chem Soc Rev* 43:6555–6569. <https://doi.org/10.1039/c3cs60468c>
 24. Shi Y, Zhang B (2016) Recent advances in transition metal phosphide nanomaterials: synthesis and applications in hydrogen evolution reaction. *Chem Soc Rev* 45:1529–1541. <https://doi.org/10.1039/c5cs00434a>
 25. Shen W, Wu B, Liao F et al (2017) Optimizing the hydrogen evolution reaction by shrinking Pt amount in Pt–Ag/SiNW nanocomposites. *Int J Hydrogen Energy* 42:15024–15030. <https://doi.org/10.1016/j.ijhydene.2017.03.110>
 26. Walter MG, Warren EL, McKone JR et al (2010) Solar water splitting cells. *Chem Rev* 110:6446–6473. <https://doi.org/10.1021/cr1002326>
 27. Zeng M, Li Y (2015) Recent advances in heterogeneous electrocatalysts for the hydrogen evolution reaction. *J Mater Chem A* 3:14942–14962. <https://doi.org/10.1039/c5ta02974k>
 28. Zhang G, Wang G, Liu Y et al (2016) Highly active and stable catalysts of phytic acid-derivative transition metal phosphides for full water splitting. *J Am Chem Soc* 138:14686–14693. <https://doi.org/10.1021/jacs.6b08491>
 29. Moon JS, Jang JH, Kim EG et al (2015) The nature of active sites of Ni₂P electrocatalyst for hydrogen evolution reaction. *J Catal* 326:92–99. <https://doi.org/10.1016/j.jcat.2015.03.012>
 30. Karunadasa HI, Montalvo E, Sun Y et al (2012) A molecular MoS₂ edge site mimic for catalytic hydrogen generation. *Science* 335:698–702. <https://doi.org/10.1126/science.1215868>
 31. Nørskov JK, Bligaard T, Logadottir A et al (2005) Trends in the exchange current for hydrogen evolution. *J Electrochem Soc* 152:J23. <https://doi.org/10.1149/1.1856988>
 32. Chen YW, Prange JD, Dühnen S et al (2011) Atomic layer-deposited tunnel oxide stabilizes silicon photoanodes for water oxidation. *Nat Mater* 10:539–544. <https://doi.org/10.1038/nmat3047>
 33. Fukata N, Subramani T, Jevasuwan W et al (2017) Functionalization of silicon nanostructures. *Energy Storage* 13:1701713. <https://doi.org/10.1002/sml.201701713>
 34. Morales AM, Lieber CM (1998) A Laser ablation method for the synthesis of crystalline semiconductor nanowires. *Science* 279(5348):208–211. <https://doi.org/10.1126/science.279.5348.208>
 35. Shi WS, Peng HY, Xu L et al (2000) Coaxial three-layer nanocables synthesized by combining laser ablation and thermal evaporation. *Adv Mater* 12:1927–1930. [https://doi.org/10.1002/1521-4095\(200012\)12:24%3c1927::AID-ADMA1927%3e3.0.CO;2-C](https://doi.org/10.1002/1521-4095(200012)12:24%3c1927::AID-ADMA1927%3e3.0.CO;2-C)
 36. Zhang RQ, Lifshitz Y, Lee ST (2003) Oxide-assisted growth of semiconducting nanowires. *Adv Mater* 15:635–640. <https://doi.org/10.1002/adma.200301641>
 37. Holmes JD, Johnston KP, Doty RC, Korgel BA (2000) Control of thickness and orientation of solution-grown silicon nanowires. *Science* 287(5457):1471–1473
 38. Heitsch AT, Fanfair DD, Tuan HY, Korgel BA (2008) Solution-liquid-solid (SLS) growth of silicon nanowires. *J Am Chem Soc* 130:5436–5437. <https://doi.org/10.1021/ja8011353>
 39. Bolton JR, Stricklert SJ, Connolly J (1985) Limiting and realizable efficiencies of solar photolysis of water. *Nature* 316:495–500
 40. Vargas-Hernández RA (2020) Bayesian optimization for calibrating and selecting hybrid-density functional models. *J Phys Chem A* 124:4053–4061. <https://doi.org/10.1021/acs.jpca.0c01375>
 41. Klime J, Bowler DR, Michaelides A (2011) Van der Waals density functionals applied to solids. *Phys Rev B* 83:1–13. <https://doi.org/10.1103/PhysRevB.83.195131>
 42. Verma LK (2000) Studies on methanol fuel cell. *J Power Sources* 86:464–468
 43. Luong JHT, Hrapovic S, Wang D et al (2004) Solubilization of multiwall carbon nanotubes by 3-aminopropyltriethoxysilane towards the fabrication of electrochemical biosensors with promoted electron transfer. *Electroanalysis* 16:132–139
 44. Wang Z, Liu J, Liang Q et al (2002) Carbon nanotube-modified electrodes for the simultaneous determination of dopamine and ascorbic acid. *Analyst* 127:653–658

45. Luo H, Shi Z, Li N et al (2001) Investigation of the electrochemical and electrocatalytic behavior of single-wall carbon nanotube film on a glassy carbon electrode. *Anal Chem* 73:915–920
46. Cao X, Han Y, Gao C et al (2014) Highly catalytic active PtNiCu nanochains for hydrogen evolution reaction. *Nano Energy* 9:301–308. <https://doi.org/10.1016/j.nanoen.2014.08.008>
47. Sheng W, Gasteiger HA, Shao-Horn Y (2010) Hydrogen oxidation and evolution reaction kinetics on platinum: acid vs alkaline electrolytes. *J Electrochem Soc* 157:B1529. <https://doi.org/10.1149/1.3483106>
48. Zhu L, Lin H, Li Y et al (2016) A rhodium/silicon co-electrocatalyst design concept to surpass platinum hydrogen evolution activity at high overpotentials. *Nat Commun*. <https://doi.org/10.1038/ncomms12272>
49. Zhang J, Zhao Y, Guo X et al (2018) Single platinum atoms immobilized on an MXene as an efficient catalyst for the hydrogen evolution reaction. *Nat Catal* 1:985–992
50. Hüner B, Demir N, Kaya MF (2023) Ni–Pt coating on graphene based 3D printed electrodes for hydrogen evolution reactions in alkaline media. *Fuel* 331:125971
51. Gong M, Wang D-Y, Chen C-C et al (2016) A mini review on nickel-based electrocatalysts for alkaline hydrogen evolution reaction. *Nano Res* 9:28–46
52. Vij V, Sultan S, Harzandi AM et al (2017) Nickel-based electrocatalysts for energy-related applications: oxygen reduction, oxygen evolution, and hydrogen evolution reactions. *ACS Catal* 7:7196–7225. <https://doi.org/10.1021/acscatal.7b01800>
53. Lu J, Xiong T, Zhou W et al (2016) Metal nickel foam as an efficient and stable electrode for hydrogen evolution reaction in acidic electrolyte under reasonable overpotentials. *ACS Appl Mater Interfaces* 8:5065–5069. <https://doi.org/10.1021/acami.6b00233>
54. Rao D, Wang L, Zhu Y et al (2016) Electrochemical preparation of Ni–Mo coated coral-like Cu micro-arrays for electrocatalytic hydrogen evolution reaction in acidic solution. *J Electrochem Soc* 163:H1026–H1032. <https://doi.org/10.1149/2.1021610jes>
55. Gomez Vidales A, Omanovic S (2018) Evaluation of nickel-molybdenum-oxides as cathodes for hydrogen evolution by water electrolysis in acidic, alkaline, and neutral media. *Electrochim Acta* 262:115–123. <https://doi.org/10.1016/j.electacta.2018.01.007>
56. Di HX, Xu F, Li F et al (2017) Composition-performance relationship of Ni_xCu_y nanoalloys as hydrogen evolution electrocatalyst. *J Electroanal Chem* 799:235–241. <https://doi.org/10.1016/j.jelechem.2017.05.050>
57. Shen Y, Zhou Y, Wang D et al (2018) Nickel–copper alloy encapsulated in graphitic carbon shells as electrocatalysts for hydrogen evolution reaction. *Adv Energy Mater* 8:1–7. <https://doi.org/10.1002/aenm.201701759>
58. Shen Y, Lua AC, Xi J, Qiu X (2016) Ternary platinum–copper–nickel nanoparticles anchored to hierarchical carbon supports as free-standing hydrogen evolution electrodes. *ACS Appl Mater Interfaces* 8:3464–3472. <https://doi.org/10.1021/acami.5b11966>
59. Wan L, Zhang J, Chen Y et al (2017) Varied hydrogen evolution reaction properties of nickel phosphide nanoparticles with different compositions in acidic and alkaline conditions. *J Mater Sci* 52:804–814. <https://doi.org/10.1007/s10853-016-0377-7>
60. Larbi KK, Barati M, McLean A (2011) Reduction behaviour of rice husk ash for preparation of high purity silicon. *Can Metall Q* 50:341–349
61. Barati M, Sarder S, McLean A, Roy R (2011) Recovery of silicon from silica fume. *J Non-Cryst Solids* 357:18–23
62. Larbi KK (2010) Synthesis of High Purity Silicon from Rice Husks; Master of Applied Science, Department of Materials Science and Engineering, University of Toronto
63. Shyu JZ, Otto K (1988) Identification of platinum phases on γ -alumina by XPS. *Appl Surf Sci* 32:246–252
64. Dupin J-C, Gonbeau D, Vinatier P, Levasseur A (2000) Systematic XPS studies of metal oxides, hydroxides and peroxides. *Phys Chem Chem Phys* 2:1319–1324
65. Sirtori V, Lombardi L, Cavallotti PL, Magagnin L (2003) Determination of correct composition in nickel–phosphorus films by XPS angle resolved technique. *Appl Surf Sci* 217:163–169
66. de Souza MO, Mendes FMT, de Souza RF, dos Santos JHZ (2004) XPS characterization of nickel-acetylacetonate impregnated in NaX and NaY zeolites. *Microporous Mesoporous Mater* 69:217–221
67. Biesinger MC, Payne BP, Lau LWM et al (2009) X-ray photoelectron spectroscopic chemical state quantification of mixed nickel metal, oxide and hydroxide systems. *Surf Interface Anal* 41:324–332
68. Şen F, Gökağaç G (2007) Different sized platinum nanoparticles supported on carbon: an XPS study on these methanol oxidation catalysts. *J Phys Chem C* 111:5715–5720
69. Yang J, Lu S, Kan S et al (2009) Electrochemical preparation of silicon nanowires from nanometre silica in molten calcium chloride. *Chem Commun*. <https://doi.org/10.1039/b902029b>
70. Abouatallah RM, Kirk DW, Thorpe SJ, Graydon JW (2001) Reactivation of nickel cathodes by dissolved vanadium species during hydrogen evolution in alkaline media. *Electrochim Acta* 47:613–621
71. Huot JY, Brossard L (1987) Time dependence of the hydrogen discharge at 70 C on nickel cathodes. *Int J Hydrogen Energy* 12:821–830
72. Rommal HEG, Moran PJ (1985) Time-dependent energy efficiency losses at nickel cathodes in alkaline water electrolysis systems. *J Electrochem Soc* 132:325
73. Laursen AB, Varela AS, Dionigi F et al (2012) Electrochemical hydrogen evolution: Sabatier’s principle and the volcano plot. *J Chem Educ* 89:1595–1599
74. Sarkar S, Peter SC (2018) An overview on Pd-based electrocatalysts for the hydrogen evolution reaction. *Inorg Chem Front* 5:2060–2080
75. Sial MAZG, Mateen M, Naz R et al (2023) Alloying platinum single atoms with nickel iron nanoalloys for high performance hydrogen evolution reaction. *Int J Hydrogen Energy*. <https://doi.org/10.1016/j.ijhydene.2023.06.291>
76. Mu R, Fu Q, Xu H et al (2011) Synergetic effect of surface and subsurface Ni species at Pt–Ni bimetallic catalysts for CO oxidation. *J Am Chem Soc* 133:1978–1986
77. Zoski CG (2007) Handbook of Electrochemistry. <https://doi.org/10.1016/B978-044451958-0.50000-8>
78. Anantharaj S, Kundu S (2019) Do the evaluation parameters reflect intrinsic activity of electrocatalysts in electrochemical water splitting? *ACS Energy Lett* 4:1260–1264
79. Roy SB, Akbar K, Jeon JH, Jerng S-K, Truong L, Kim K, Yi Y, Chun S-H (2019) Iridium on vertical graphene as an all-round catalyst for robust water splitting reactions. *J Mater Chem A* 7:20590–20596
80. Lasia A (2014) Electrochemical impedance spectroscopy and its applications. Springer, New York. <https://doi.org/10.1007/978-1-4614-8933-7>
81. Yang L, Lu S, Wang H et al (2017) The self-activation and synergy of amorphous Re nanoparticle–Si nanowire composites for the electrocatalytic hydrogen evolution. *Electrochim Acta* 228:268–273
82. Ensafi AA, Ghadirian F, Jafari-Asl M, Rezaei B (2018) WS₂ grafted on silicon and nano-silicon particles etched: a high-performance electrocatalyst for hydrogen evolution reaction. *J Iran Chem Soc* 15:613–620

83. Khdary NH, Ghanem MA, Abdelsalam ME et al (2019) Copper–Ni–SiO₂ nanoparticles catalyst for hydrogen evolution reaction. *Int J Hydrogen Energy* 44:22926–22935
84. Eiler K, Suriñach S, Sort J, Pellicer E (2020) Mesoporous Ni-rich Ni–Pt thin films: electrodeposition, characterization and performance toward hydrogen evolution reaction in acidic media. *Appl Catal B* 265:118597
85. Cui M, Wang F, Zhao W et al (2023) Plasma-synthesized platinum single atom and nanoparticle catalysts for high-current-density hydrogen evolution. *Chem Eng J* 460:141676
86. Jiang G, Zhang C, Liu X et al (2022) Electrocatalytic hydrogen evolution of highly dispersed Pt/NC nanoparticles derived from porphyrin MOFs under acidic and alkaline medium. *Int J Hydrogen Energy* 47:6631–6637
87. Chen T, Ye B, Dai H et al (2021) Ni-doped CoP/Co₂P nanospheres as highly efficient and stable hydrogen evolution catalysts in acidic and alkaline mediums. *J Solid State Chem* 301:122299
88. Du Z, Wang Y, Li J, Liu J (2019) Facile fabrication of Pt–Ni alloy nanoparticles supported on reduced graphene oxide as excellent electrocatalysts for hydrogen evolution reaction in alkaline environment. *J Nanopart Res* 21:1–15
89. Xu W, Chang J, Cheng Y et al (2022) A multi-step induced strategy to fabricate core-shell Pt–Ni alloy as symmetric electrocatalysts for overall water splitting. *Nano Res* 15:965–971
90. Fu M, Zhang Q, Sun Y et al (2020) Ni–Fe nanocubes embedded with Pt nanoparticles for hydrogen and oxygen evolution reactions. *Int J Hydrogen Energy* 45:20832–20842
91. Lasia A (2002) Electrochemical impedance spectroscopy and its applications. In: *Modern aspects of electrochemistry*. Springer, pp 143–248
92. Shi H, Liu L, Shi Y et al (2019) Silicon monoxide assisted synthesis of Ru modified carbon nanocomposites as high mass activity electrocatalysts for hydrogen evolution. *Int J Hydrogen Energy* 44:11817–11823

Publisher's Note Springer Nature remains neutral with regard to jurisdictional claims in published maps and institutional affiliations.

Authors and Affiliations

Merna N. Elsodany¹ · M. A. Abdel Rahim¹ · Nasser H. Shalaby² · M. A. Sultan¹

✉ M. A. Sultan
sultan@sci.cu.edu.eg; m.a.sultan20060@gmail.com;
m_a_sultan2006@yahoo.com

² Egyptian Petroleum Research Institute, 1 Ahmed El-Zomor St., Nasr City, Cairo 11727, Egypt

¹ Department of Chemistry, Faculty of Science, University of Cairo, Giza 12613, Egypt